Ultramicroscopy 111 (2011) 887–893

Contents lists available at ScienceDirect

Ultramicroscopy

journal homepage: www.elsevier.com/locate/ultramic

A holographic biprism as a perfect energy filter?

Jo Verbeeck [a,*], Giovanni Bertoni [b], Hannes Lichte [c]

[a] EMAT, University of Antwerp, Groenenborgerlaan 171 B-2020, Antwerp, Belgium
[b] Italian Institute of Technology (IIT), via Morego 30, IT-16163 Genoa, Italy
[c] Triebenberglabor, Dresden University, D-01062 Dresden, Germany

ARTICLE INFO

Available online 4 February 2011

Keywords:
Holography
Inelastic scattering
Coherence
EELS

ABSTRACT

It has often been stated that a holographic biprism represents a near perfect energy filter and only elastically scattered electrons can participate in the interference fringes. This is based on the assumption that the reference wave does not contain inelastically scattered electrons. In this letter we show that this is not exactly true because of the delocalised inelastic interaction of the reference wave with the sample. We experimentally and theoretically show that inelastic scattering plays a role in the fringe formation, but it is shown that this contribution is small and can usually be neglected in practice.

1. Introduction: electron interference

Assume an electron biprism (Möllenstedt and Düker, [1]) illuminated by a plane wave propagating in z-direction

$$\Psi(\mathbf{r},z;t) = ae^{i2\pi kz}e^{i\omega t} \tag{1}$$

with amplitude a, wavenumber $k=1/\lambda$ at wavelength λ, and frequency ω. The vector $\mathbf{r}=(x,y)$ defines a position in a plane perpendicular to the electron propagation direction z. The wave is split in two partial waves passing on the right and the left, which, by virtue of the electric field around the biprism filament, are deflected by a very small angle γ towards each other resulting in

$$\Psi_1(\mathbf{r},z;t) = a_1e^{i2\pi\mathbf{k}_\perp\cdot\mathbf{r}}e^{i2\pi k_z z}e^{i\omega t} \quad \text{for } x<0 \tag{2}$$

$$\Psi_2(\mathbf{r},z;t) = a_2e^{-i2\pi\mathbf{k}_\perp\cdot\mathbf{r}}e^{i2\pi k_z z}e^{i\omega t} \quad \text{for } x>0 \tag{3}$$

with $k_\perp \approx k\beta/2$, $k_z \approx k$ and the biprism running along the y direction (Fig. 1).

Some distance downstream the biprism filament, the two tilted waves are mutually shifted laterally hence are superimposed under a shear s; this means that in the point $\mathbf{r}$ of the detector we find superimposed the points $\mathbf{r_1}=\mathbf{r}-s/2\mathbf{e_x}$ and $\mathbf{r_2}=\mathbf{r}+s/2\mathbf{e_x}$ of the two waves with $\mathbf{e_x}$ the unit vector in x direction. The superimposed waves form a cosinoidal interference pattern

$$I(\mathbf{r}) = a_1^2+a_2^2+2a_1a_2\cos(2\pi q_c\mathbf{r}\cdot\mathbf{e_x}) \tag{4}$$

with the spatial frequency $q_c=k\beta$ given by the angle β of the superposition.

By definition, the two waves are fully coherent with each other, since they arise by wavefront splitting from one and the same wave. However, there is a problem in that this wave only accommodates one electron, which gives rise to a point-like impact on the detector not showing an extended interference pattern. The point of impact is unpredictable, however, a posteriori well localizable on the detector. The probability of impact at a certain position is governed by the interference of the wave function. To fill the probability distribution with events, the experiment is done with many electrons emitted from the source during the exposure time. The waves of these electrons emitted from different source points and at different energies are mutually incoherent, i.e. they do not have a fixed phase relation. Nevertheless, they produce similar interference patterns only slightly shifted aside according to the emitting positions in the source and with only slightly different spatial frequencies q_c from the different energies. Summing up the intensities of all electrons, one ends up with the intensity distribution

$$I(\mathbf{r}) = a_1^2+a_2^2+2a_1a_2|\mu_{ill}|\cos(2\pi q_c\mathbf{r}\cdot\mathbf{e_x}). \tag{5}$$

This is very similar to the single-electron interference, except for the degree of coherence of illumination

$$\mu_{ill}(s,x) = |\mu_{ill}(s,x)|e^{i\rho(s,x)}, \tag{6}$$

which dampens the contrast by $|\mu_{ill}(s,x)|$ and produces a fringe shift $\rho(s,x)$, depending on shear s and the coordinate x, i.e. the order of interference. For common electron sources, it can be factorized with a spatial and a temporal coherence function

$$\mu_{ill}(s,x) = \mu^{sc}(s)\mu^{tc}(x) \tag{7}$$

* Corresponding author.
E-mail address: jo.verbeeck@ua.ac.be (J. Verbeeck).

0304-3991/$ - see front matter © 2011 Elsevier B.V. All rights reserved.
doi:10.1016/j.ultramic.2011.01.042

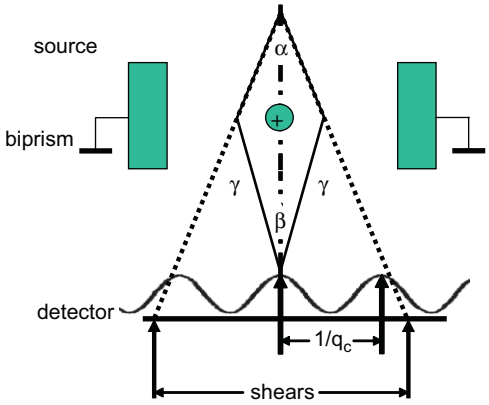

Fig. 1. Setup for electron biprism interference. The electrons passing the thin biprism filament on the right and the left are deflected by an angle $\pm\gamma$ by virtue of the electric field around the positively charged filament; they superimpose at an angle β downstream on the detector. The deflection gives rise to a lateral displacement of the two waves such that they overlap at the shear s.

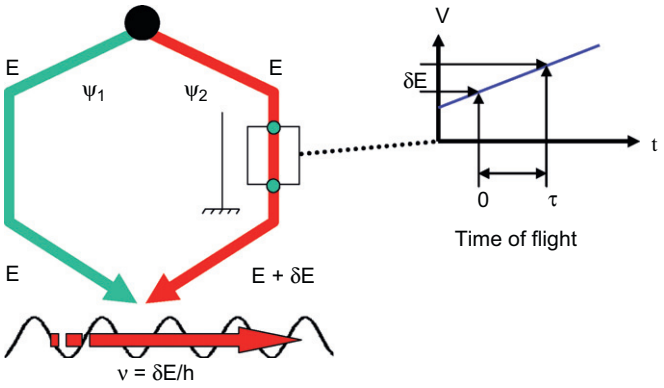

Fig. 2. Electron interference of two coherent partial waves with a mutual energy difference δE. The energy of the left wave going through vacuum remains unchanged. The energy of the right wave running through a tube with a ramped electric potential picks up an energy δE. The interference pattern is moving at a beat frequency $\nu=\delta E/h$.

which are given as Fourier transforms of the intensity distribution and energy spectrum of the electron source, respectively. For details, see [2]. In any case, μ_{ill} is a property of the electron ensemble collected during the exposure time; it says nothing about the coherence properties of the single-electron events. In the following we assume $\mu_{ill}(s,x)=1$.

1.1. Energy difference between superimposed partial waves

As shown by Schmid [3], one can generate an energy difference δE between the two partial waves. Then the waves read as

$$\Psi_1(\mathbf{r},z;t)=a_1e^{i2\pi\mathbf{k}_\perp\cdot\mathbf{r}}e^{i2\pi k_z z}e^{i\omega_1 t} \tag{8}$$

$$\Psi_2(\mathbf{r},z;t)=a_2e^{-i2\pi\mathbf{k}_\perp\cdot\mathbf{r}}e^{i2\pi k_z z}e^{i\omega_2 t} \tag{9}$$

with $\delta\omega=\omega_1-\omega_2=\delta E/\hbar$. The tiny change of q_c with δE can safely be neglected. The main point is that the resulting interference pattern is now time-dependent:

$$I(\mathbf{r})=a_1^2+a_2^2+2a_1a_2\cos(2\pi q_c\mathbf{r}\cdot\mathbf{e_x}+\delta\omega t). \tag{10}$$

In that there is a time-dependent phase $\phi(t)=\delta\omega t$, and hence the fringes move sideways at a velocity given by $\dot{x}=\dot{\phi}/2\pi q_c=\delta E/hq_c$. Therefore, at a fixed detector position, we measure a beat of intensity with a frequency $\nu=\delta E/h$ (Fig. 2).

During the exposure time τ, the intensity distribution

$$I_{\delta E}(x)=2\left[\tau+\int_0^\tau\cos(2\pi q_c x+\phi(t))\,dt\right] \tag{11}$$

$$=2\tau[1+|\mu_{\delta E}|\cos(2\pi q_c x+\phi(\tau/2))] \tag{12}$$

with

$$\mu_{\delta E}(\tau)=\frac{1}{\tau}\int_0^\tau e^{i\phi(t)}\,dt \tag{13}$$

$$=|\mu_{\delta E(\tau)}|e^{i\phi(\tau/2)} \tag{14}$$

This can be seen as an additional degree of coherence between the superimposed partial waves, which describes the effect of the possible inelastic events in one of the ray paths. Inserting the above $\phi(t)$, one obtains

$$|\mu_{\delta E}(\tau)|=\frac{\sin\left(\frac{\delta E}{\hbar}\tau\right)}{\frac{\delta E}{\hbar}\tau}. \tag{15}$$

For an appreciable fringe contrast, $\delta E\ll\hbar/\tau$ is needed. At the usual exposure time of $\tau=1$ s, this results in $\delta E<10^{-15}$ eV. Therefore, we consider $\delta E\approx10^{-15}$ eV as the threshold above which no coherence can be measured in practical electron holography experiments [5,6].

2. Electron holography

2.1. Elastic interaction

Accordingly, we talk about elastic interaction, if the electron energy before and behind the specimen is the same on the scale of 10^{-15} eV. Assume that amplitude $a_{obj}(x,y)$ and phase

$$\phi_{object}(x,y)=\frac{e}{\hbar v}\int_{path}V(x,y,z)+vA_z(x,y,z)\,dz \tag{16}$$

have been modulated by elastic interaction with the electric potential $V(x,y,z)$ and the z-component of the magnetic vector potential $A_z(x,y,z)$ along the trajectory of the fast electron through the object (the Aharanov–Bohm effect [4]); v is the electron velocity. With the biprism oriented along y-direction, a plane reference wave $\psi_{ref}=a_{ref}$ is superimposed to the object exit wave $\psi_{obj}=a_{obj}(x,y)e^{i\phi_{obj}(x,y)}$. Then a hologram intensity results as

$$I_{hol}(x,y)=a_{ref}^2+a_{obj}^2+2|\mu_{ill}|a_{ref}a_{obj}\cos(2\pi q_c x+\phi_{obj}(x,y)). \tag{17}$$

From the hologram, the object wave may be reconstructed completely in amplitude and phase, however, dampened by the degree of coherence μ_{ill} in the incoming beam.

2.2. Inelastic interaction

Now consider also inelastic interaction creating e.g. phonons (≈10 meV), plasmons (≈10 eV) or inner shell excitations (≈100 eV) in the object area. Assume that the reference wave passing by the object does not experience any energy loss. Then, from the above derived destruction of coherence for $\delta E>10^{-15}$ eV, it is intuitively clear that these "inelastic" electrons in the object area do not form interference fringes with the elastic ones in the reference wave; instead, they end up in the background and reduce the contrast of the hologram and the amplitude of the wave reconstructed from it; this is compulsory for all known inelastic processes mentioned above, since $\delta E\leq10^{-15}$ eV is a necessary condition. Therefore, only elastic electrons build up any reconstructed wave from the hologram. In this sense, electron holography acts as a (nearly) perfect energy filter [5,6].

The question remains, whether inelastically scattered electrons can produce interference contrast, if both paths have suffered exactly the same energy loss within $\delta E < 10^{-15}$ eV. For this, we have to look at the process of inelastic interaction in more detail. In simple words, the initial wave of an electron collapses by inelastic interaction, which may be considered a measuring process, and a new one is generated corresponding to the new energy of the inelastic electron. This wave represents a state orthogonal to the previous one; orthogonality is equivalent to attributing a random phase to it, which, in addition to $\mu_{\delta E}$, destroys phase coherence with the remaining elastic waves. The new inelastic wave on the other hand can of course still show partial coherence with itself.

For investigation of the emerging new wave, the coherence properties within the inelastic wave field of plasmon scattered electrons were studied by means of superimposing different parts of the inelastic waves with a biprism: Using an Ω-imaging filter microscope (Carl-Zeiss, LaB6-gun), some coherence was found (Harscher, Lichte and Meyer, [7]); with improved instrumentation (Philips CM30 FEG and GIF, Lichte and Freitag [8]), the width of the coherence area was estimated to be larger than 10 nm. Finally, in a more elaborated experiment, the degree of coherence was measured as a function of shear produced by the biprism between the inelastic partial waves (Verbeeck et al. [9], Potapov et al. [10]). Surprisingly, it was also found that electrons passing the edge of the specimen at some nm distance in vacuum ("aloof-excitation"), also show a remarkably good degree of coherence [10].

All these experiments seem to contradict the intuitive concept of the biprism as a perfect energy filter, in particular the aloof-excitation, because also the reference wave is affected by delocalised inelastic interaction. On top of this, these experiments raise the question as to what extent conventional off-axis holography is influenced by inelastic scattering.

2.3. Delocalised inelastic interaction

The discrepancy between the experiments showing clear indications of coherence for energy losses of tens of eV and the theory stating that a biprism is a nearly perfect energy filter was resolved by Schattschneider et al. [11] and Verbeeck et al. [9] by taking into account the delocalised interaction of the fast electrons with the sample using a theory based on the mixed dynamic form factor presented by Rose et al. [12] and by Schattschneider et al. [11,13].

To understand the effect of delocalised interaction we refer to a typical holographic setup as sketched in Fig. 3 where the biprism voltage determines the so-called 'shear' value s. The location of the sample with respect to the biprism wire can be denoted as the 'offset' d. Combining this setup with an energy filter allows to study the formation of fringes in case of inelastic scattering.

The crucial point is that both arms of the interferometer can excite an inelastic event in the sample in location r due to their long range Coulomb interaction V_{1r} and V_{2r}. Of course the scattering probability decays with the distance of both arms to the scattering center but a certain part of the electrons will still create fringes due to the fact that both arms have excited the same scattering event.

In this paper we will first present experimental evidence that this is indeed happening and we will study the dependence on the offset d and the energy loss δE. Finally we will present the theory to understand this effect which will be compared to our experimental findings. The theory can than be used to make estimates on how much inelastic scattering is present in a typical off-axis reconstructed hologram.

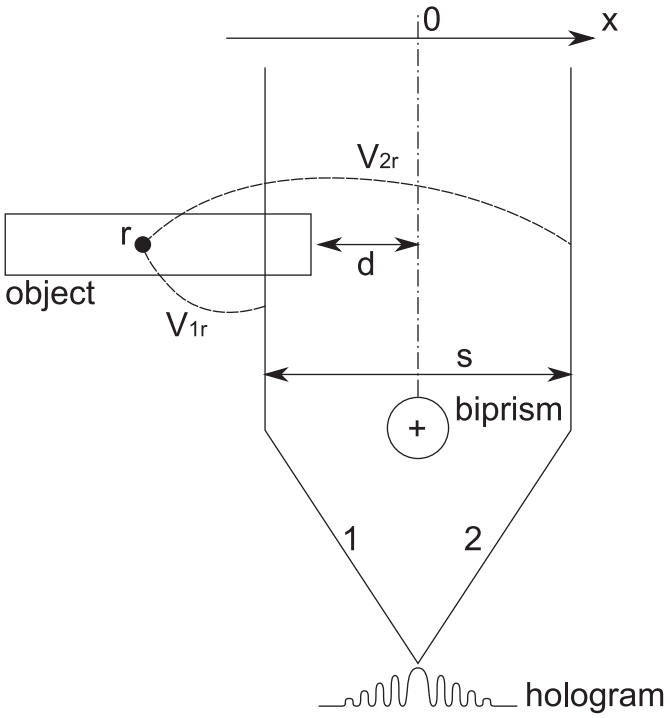

Fig. 3. Sketch of the holography setup showing the shear value s and the offset d. Each arm of the interferometer can act nonlocally with a scattering center in r via the interaction potential V_{1r} and V_{2r}.

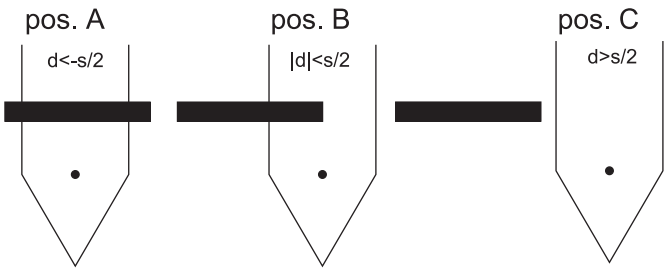

Fig. 4. Sketch of the three different experimental situations. In pos. A both arms of the interferometer pass through the sample. In pos. B only one arm goes through the sample while in pos. C the sample does not intersect with the arms of the interferometer.

3. Experiments

Experiments were carried out on a polycrystalline Al foil prepared with electrochemical polishing on a Philips CM30 microscope operating at 300 kV equipped with a biprism and a GIF 200 energy filter. Fringe patterns were recorded with a fixed shear value of 28 nm in the plane of the sample. Different positions of the sample edge with respect to the biprism are taken (Fig. 4) and energy filtered fringe patterns are recorded at 0, 5, 10 and 15 eV with an energy selecting slit of 5 eV. The estimated positions of the sample edge with respect to the biprism wire are $d=-20$, -9, and 5 nm for pos. A, B, and C, respectively. A final interference pattern is recorded with the energy selecting slit open so that all electrons can participate. A set of intensity profiles over the fringe region is shown in Fig. 5 for the different energy losses. It is obvious from these recordings that fringes are visible for all energy losses, showing clearly the breakdown of the intuitive concept of the biprism as a perfect energy filter since in that case we would only see fringes for

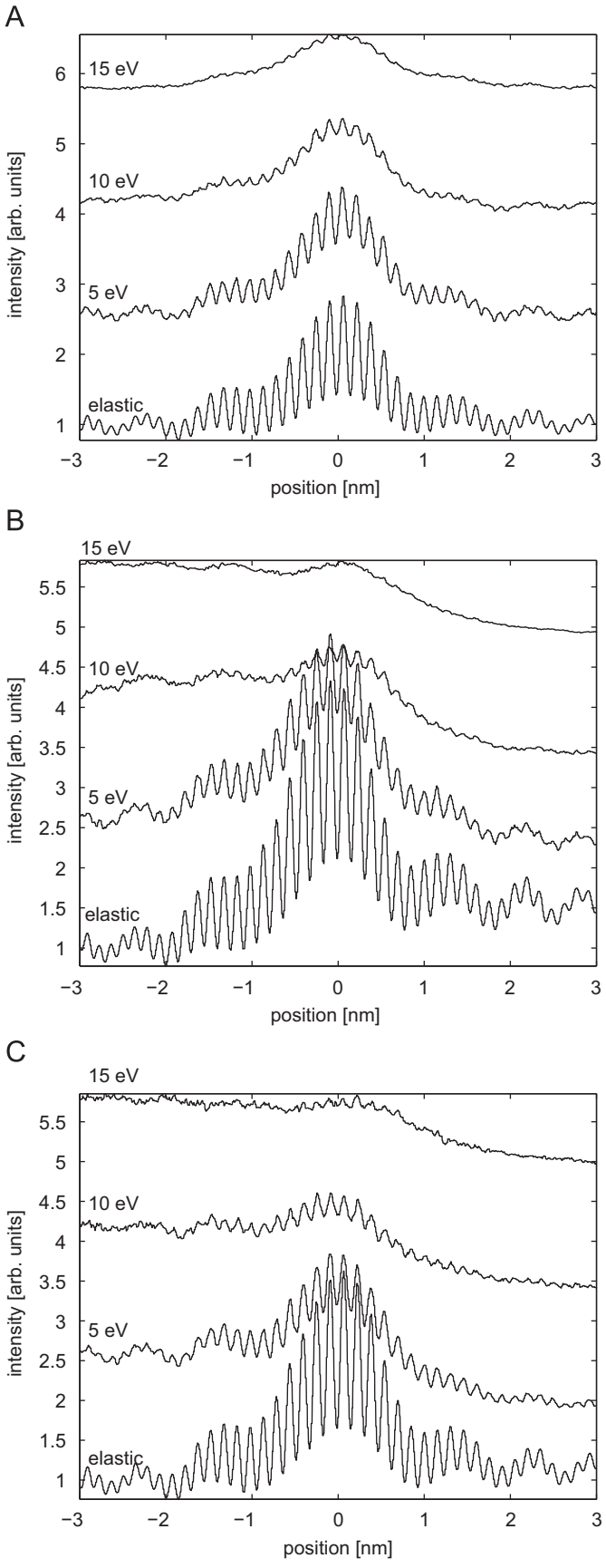

Fig. 5. Experimental fringe patterns as a function of energy loss for three distinct situations and three energy losses (graphs shifted vertically for clarity): (A) Sample–sample interference, (B) vacuum–sample interference as in usual off-axis holography, and (C) vacuum–vacuum interference as in the aloof-excitation setup.

elastic electrons. Quantifying the fringe contrast in a selected region and normalising it to the fringe contrast in the elastically filtered case (ZL, $\mu_{ill} \approx 0.4$, no objective aperture) we get Table 1. We observe a strong reduction in contrast with increasing energy loss that is more pronounced when the specimen is overlapping the biprism wire (pos. A) and becomes rather small for a specimen position that is far away from the biprism (pos. C). The total contrast in the unfiltered case is of course lower than the filtered case because inelastically scattered electrons contribute that have a lower contrast. The contrast difference between the zero loss filtered and unfiltered experiment is smaller for pos. C, which can be understood as the effect that the proportion of inelastic scattering in the pattern is greatly reduced with distance to the sample and the contrast of the fringes generated by these inelastic electrons is higher.

To quantify this, we can study the amplitude of the fringes tabulated in Table 2. Here we normalised the amplitude to the total unfiltered amplitude. From the table we see that most of the fringe amplitude is coming from elastic electrons (ZL) more so when the specimen is further away from the biprism (pos. C). The inelastic signal is consequently reduced as the energy loss increases and as the distance to the biprism increases. Table 3 gives the probability of scattering into a certain energy range which depends on the thickness of the sample and on the distance to the biprism. We use an integration window of 5 eV centered around the nominal loss and normalise the total intensity to 1. The inelastic scattering probability is of course higher than the amplitude since the inelastically scattered electrons are only partially coherent.

Table 1
Fringe contrast normalised to the zero loss filtered pattern as a function of energy loss and position with respect to the biprism.

δE	Pos. A	Pos. B	Pos. C
ZL	1.0000	1.0000	1.0000
5 eV	0.5100	0.5778	0.5039
10 eV	0.1799	0.2710	0.3801
15 eV	0.0608	0.0989	0.1682
Total	0.8403	0.9500	0.9818

Table 2
Fringe amplitude normalised to the total amplitude in the unfiltered pattern as a function of energy loss and position with respect to the biprism.

δE	Pos. A	Pos. B	Pos. C
ZL	0.9703	0.9812	0.9882
5 eV	0.0199	0.0155	0.0091
10 eV	0.0087	0.0048	0.0026
15 eV	0.0081	0.0027	0.0009
Total	1.0000	1.0000	1.0000

Table 3
Scattering probability normalised to the total signal in the unfiltered pattern as a function of energy loss and position with respect to the biprism.

δE	Pos. A	Pos. B	Pos. C
ZL	0.8153	0.9321	0.9702
5 eV	0.0329	0.0254	0.0177
10 eV	0.0408	0.0168	0.0068
15 eV	0.1114	0.0261	0.0054
Total	1.0000	1.0000	1.0000

Note that from these tables we can also conclude that the effect we are studying is not caused by the energy spread of the incoming electrons since that effect would be independent on the distance to the biprism. Taking a zero loss peak under the same conditions we get a contribution to the scattering probability of 97%, 1.6%, 0.36%, 0.22% for an energy selecting slit of 5 eV at 0, 5, 10 and 15 eV. Comparing this to Table 3 we see that this contribution is only significant for energy losses of 5 eV and especially for pos. C.

These experimental observations clearly show that a biprism is not a perfect energy filter, since inelastic fringes are present even in the case where a reference wave is overlapping with a specimen wave (pos. C). The reason for this is the delocalised interaction which becomes stronger at lower energy losses. This delocalisation leads to inelastic scattering in the region outside the sample through long range Coulomb interaction. So although the specimen is geometrically not present on one side of the biprism, there is still delocalised inelastic interaction. The details of the interaction will be treated in the next section but we will show that the term responsible for the interference decays slower with distance as compared to the so-called direct terms. This leads to an *increasing* contrast while the amplitude decreases rapidly with distance to the sample. This observation is very similar to the aloof experiment reported by Potapov et al. [10].

4. Theory

The concept of delocalisation and coherence has been treated in great detail in [9,13]. Applying the mathematical concepts of these papers we can simulate the expected contrast as a function of energy loss and distance of the specimen edge to the biprism wire. We neglect the effect of Fresnel fringes here to keep the theory clear but we include the effect in the simulations presented in Fig. 5 as described in [14].

We start from the fact that the density matrix after inelastic scattering is given as a convolution of the mixed dynamic form factor S, describing the sample details, and the effect of the Coulomb interaction described by the modified Bessel function of the second kind, K_0 (Eq. (30) in [13]):

$$\rho(\mathbf{r},\mathbf{r}') = S(\mathbf{r},\mathbf{r}') \otimes K_0(q_E|r|)K_0(q_E|r'|). \tag{18}$$

with q_E the effective scattering vector given by the difference between the incoming (k_0) and outgoing (k') wave vector. The position vectors $\mathbf{r}=(x,y)$ and $\mathbf{r}'=(x',y')$ are chosen in the exit plane of the specimen, perpendicular to the optical axis of the microscope. Assuming a half plane sample ($x>0$) of incoherent scattering centers we can write:

$$S(\mathbf{r},\mathbf{r}') = \Pi(x)\Pi(x')\delta(\mathbf{r}-\mathbf{r}'), \tag{19}$$

with Π a step function which is one when $x>0$. The density matrix of the fast electrons becomes

$$\rho(\mathbf{r_1},\mathbf{r}'_1) = \int_{-\infty}^{\infty} \Pi(x-x_1)K_0(q_E|r|) \times \left[\int_{-\infty}^{\infty} \Pi(x'-x'_1)K_0(q_E|r'|)\delta(\mathbf{r}-\mathbf{r_1}-\mathbf{r}'+\mathbf{r}'_1)\,dr'\right] d\mathbf{r} \tag{20}$$

with $\mathbf{r_1}$ and $\mathbf{r}'_1$ two coordinates in the exit plane of the specimen. The y-integral leads to:

$$F(x,s) = \int_{-\infty}^{\infty} K_0\left(q_E\sqrt{x^2+y^2}\right)K_0\left(q_E\sqrt{(x-s)^2+y^2}\right)\,dy. \tag{21}$$

With $s=\mathbf{x1}-\mathbf{x1}'$. To include the effect of a Bohm–Pines cut-off angle [15], we use a truncated K_0 function as described in [9] instead of the full K_0 function which goes to infinity at the origin. The function $F(x,0)$ is shown in Fig. 6 for three different energy losses.

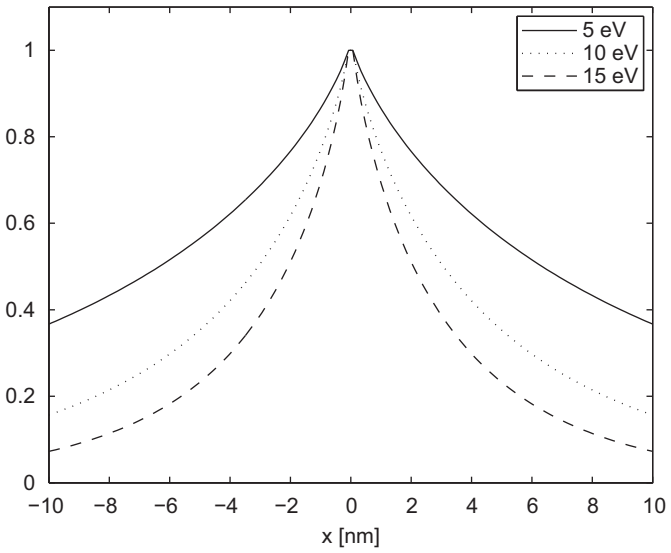

Fig. 6. $F(x,0)$ for three different energy losses and $E_0=300$ kV.

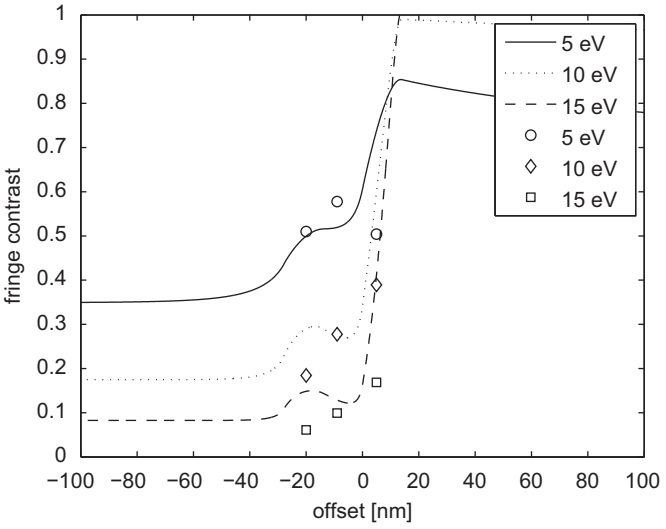

Fig. 7. Approximated relative contrast of inelastic fringes for a shear of $s=28$ nm and $E_0=300$ kV (lines) compared to the experimental values (symbols) from Table 1.

To obtain the fringe contrast we compare the off-diagonal elements of the density matrix with the two direct terms. Assuming a biprism along the y direction, the contrast becomes by symmetry independent on the y-coordinate ($s=x_1-x'_1, y_1=y'_1$). The direct terms lead to:

$$\rho(x_1,x_1) = \int_{x_1}^{\infty} F(x,0)\,dx. \tag{22}$$

The off-diagonal elements become

$$\rho(x_1+s/2,x_1-s/2) = \int_{x_1+s/2}^{\infty} F(x,s)\,dx. \tag{23}$$

The fringe contrast in position $x_1=-d$ (see Fig. 3) can be calculated as [9]

$$C(d) = \frac{2\rho(-d+s/2,-d-s/2)}{\rho(-d-s/2,-d-s/2)+\rho(-d+s/2,-d+s/2)}, \tag{24}$$

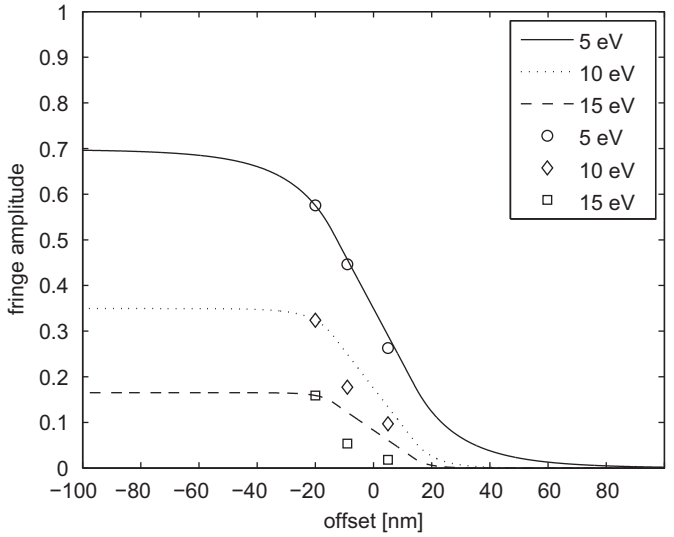

Fig. 8. Approximated relative fringe amplitude as a function of offset for a shear of $s=28$ nm and $E_0=300$ kV (lines) compared to the experimental values (symbols) from Table 2 but scaled to the $d=-20$ nm values as reference to take into account the probability of scattering.

Table 4
Estimated relative fringe amplitude assuming a scattering probability of 100% for a given energy range in a typical off-axis holography setup with $d=6.95$ nm and $s=63.9$ nm and $E_0=300$ kV. The real fringe amplitudes in an experiment can be estimated by multiplying this figure with the inelastic scattering probability in that energy range.

δE (eV)	Relative fringe amplitude (%)
5	11.3
10	1.81
15	0.267

while the fringe amplitude is given only by the off-diagonal elements [9]:

$$A(d) = 2\rho(-d+s/2,-d-s/2). \quad (25)$$

Both contrast and fringe amplitude are plotted in Figs. 7 and 8 together with the experimental data points. For the amplitude, a scaling factor based on the $d=-20$ nm experimental points is used, since the exact probability of excitation depends on the details of the sample which are unknown. A reasonable qualitative fit is obtained for both amplitude and contrast. The biggest deviation is found for pos. C ($d=5$ nm) and $\delta E=5$ eV which could be related to the influence of the contribution of the energy spread of the electrons which is highest for this point.

Note that the simulation can not be expected to contain all details because an overly simplistic constant thickness sample is assumed in the theory. Nevertheless, the theory captures the general trend and can be used to make an estimate of how much inelastic coherence will influence a more conventional high resolution off-axis holography setup. If we take a typical value for the shear $s=63.4$ nm and choose the offset to be $d=6.7$ nm (to get a fringe region of 50 nm wide with a biprism diameter of 13.4 nm related to the object plane) we can estimate the fringe amplitude for different energy regions compared to the scattering amplitude in these regions. This leads to an estimate of the fringe amplitude as presented in Table 4. In Table 4 we assume a scattering probability of 100% for each energy loss. In reality, the total scattering probability depends on the details of the sample and the experimental setup, but we can safely say that for any reasonable thickness this will be less than 10% from the elastic contribution. Taking this into account we estimate the contribution of inelastic scattering to a reconstructed hologram to be at most 1% especially for energy losses $\delta E>5$ eV. For medium resolution holography, the shear will typically be much larger ($s>100$ nm) and therefore the contribution of inelastic fringes will be even smaller.

5. Discussion

In the previous section it was clearly shown both experimentally and theoretically that inelastic scattering does contribute to the interference fringes obtained in electron holography. The fringe amplitude is typically quite low and depends mainly on three parameters:

- Energy loss δE: the higher the loss, the lower the fringe contrast. There are two reasons for this. First the amplitude decreases as higher losses are typically less likely to occur. Secondly, the contrast decreases due to a blurring by the Lorentzian distribution of the inelastic scattering. This dependency is nicely predicted by Schattschneider and Lichte [13].
- Shear s: the higher the shear the lower the contrast. This is also well predicted by the truncated K_0 function as e.g. in [9].
- Offset d: As the offset increases, the contrast *increases* due to delocalised interaction (as e.g. in Potapov et al. [10]). But at the same time the amplitude strongly decreases because of the details of delocalisation.

Note that in a typical off-axis hologram the offset is close to $d=0$ but the fringe region has a certain width given by the shear s. This will make the contribution of inelastic fringes higher on the side of the specimen as opposed to the side of the reference wave.

6. Conclusion

We have shown both experimentally and theoretically that delocalised inelastic interaction requires to change the notion of the biprism as a perfect energy filter. In all practical situations, the inelastically scattered electrons are forming part of the fringe contrast and should therefore be taken into account when comparing holographically reconstructed exit waves to theory. On the other hand this contribution is relatively small and definitely much smaller than the effect in e.g. HRTEM focal series reconstruction. The contribution to the fringe amplitude reduces rapidly with distance of the sample to the biprism wire, which for all practical cases of off-axis holography leads to a small inelastic contribution to the fringe contrast. We estimated that less than 1% of a reconstructed exit wave in off-axis holography is due to inelastically scattered electrons with an energy loss $\delta E>5$ eV. This leads to the conclusion that although the statement that a biprism is a perfect energy filter is clearly incorrect, in practice this is a reasonable assumption for energy losses above a few eV.

Acknowledgements

G.B. acknowledges the FWO-Vlaanderen for financial support under contract no. G.0147.06. J.V. and H.L. acknowledge the financial support from the European Union under the Framework 6 program under a contract for an Integrated Infrastructure Initiative. Reference 026019 ESTEEM.

References

[1] G. Möllenstedt, H. Düker, Zeitschrift für Physik 145 (1956) 377–397.
[2] H. Lichte, M. Lehmann, Rep. Prog. Phys. 71 (2008) 016102. doi:10.1088/0034-4885/71/1/016102 (46pp).
[3] H. Schmid, Ein Elektronen-Interferometer mit 300 μm weit getrennten kohärenten Teilbündeln zur Erzeugung hoher Gangunterschiede und Messung der Phasenschiebung durch das magnetische Vektorpotential bei metallisch abgeschirmtem Magnetfluß. Thesis, University of Tübingen, 1985.
[4] Y. Aharonov, D. Bohm, Significance of electromagnetic potentials in quantum theory, Phys. Rev. 115 (1959) 485–491.
[5] D. Van Dyck, H. Lichte, J.C.H. Spence, Ultramicroscopy 81 (2000) 187–194.
[6] J.C.H. Spence, J.M. Zuo, Ultramicroscopy 69 (1997) 185–190.
[7] A. Harscher, H. Lichte, J. Meyer, Interference experiments with energy filtered electrons, Ultramicroscopy 69 (1997) 201–209.
[8] H. Lichte, B. Freitag, Ultramicroscopy 81 (2000) 177–186.
[9] J. Verbeeck, D. Van Dyck, H. Lichte, P. Potapov, P. Schattschneider, Plasmon holographic experiments: theoretical framework, Ultramicroscopy 102 (2005) 239–255.
[10] P. Potapov, J. Verbeeck, P. Schattschneider, H. Lichte, D. Van Dyck, Inelastic electron holography as a variant of the Feynman thought experiment, Ultramicroscopy 107 (2007) 559–567.
[11] P. Schattschneider, H. Lichte, Phys. Rev. B 71 (2005) 045130.
[12] H. Rose, Ultramicroscopy 15 (1984) 173–192.
[13] P. Schattschneider, M. Nelhiebel, B. Jouffrey, Phys. Rev. B 59 (1999) 10959.
[14] J. Verbeeck, G. Bertoni, P. Schattschneider, Ultramicroscopy 108 (3) (2008) 263–269.
[15] G. Bertoni, J. Verbeeck, F. Brosens, Microsc. Res. Tech., in press, doi:10.1002/jemt.20894.